Understanding losses in halide perovskite thin films

Adhyaksa, G.W.P.

Publication date
2018
Document Version
Other version
License
Other

1

Introduction and General Principles

Advances in thin-film semiconductor technology will find applications in highly efficient and low-cost photovoltaics. Hybrid-halide perovskites have emerged over the unprecedented timeframe of the last 6 years as a promising class of materials for such applications. Most notably, their solar cells have achieved power conversion efficiencies above 20 % in the laboratory basis, even though many fundamental questions still remain unanswered. Therefore for the halide perovskite thin-films to have an impact beyond the laboratory requires a systematic understanding and eliminating sources of losses. This chapter starts with the most important properties of halide perovskite thin-films in comparison with other photovoltaic semiconductors as well as some unanswered questions regarding the properties. Next, we discuss material imperfections as the sources of losses, and describing the methodology used in this thesis to identify and eliminate those losses. Finally, we provide description and important findings in each chapter to outline the overall motivation covering this thesis.

1.1 Halide perovskite thin-films

The dramatic rise of halide perovskites in photovoltiacs has caught the attention of scientists across many fields, and the initial hype has been followed by investigation of perovksite's structural, optical, and electrical properties. Perovskites offer a combination of the characteristics of inorganic and organic semiconductors: the

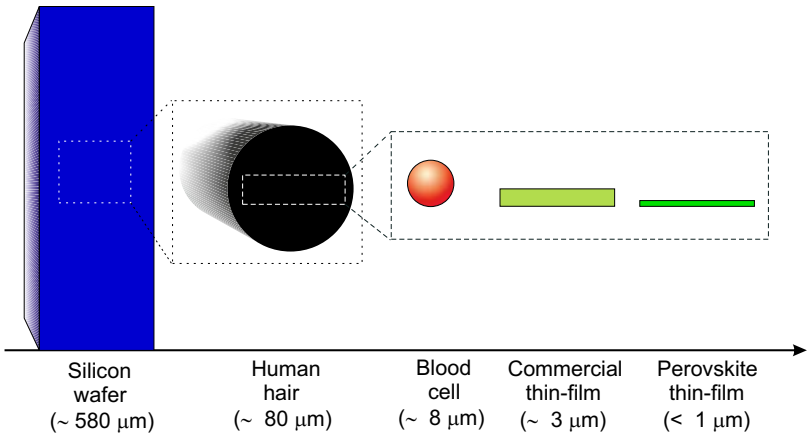

Figure 1.1: Schematic of cross-sectional scale (drawn to scale) of perovskite thin-films compared to other micron-scale relevant objects

chemical tunability of their optoelectronics properties and low-temperature and solution-based deposition recall organics; their relatively high carrier mobility, diffusion length, and radiative lifetime more resemble those of polycrystalline semiconductors (**Table 1.1**). These attractive properties have inspired dreams well beyond photovoltaics, and research in sunlight-to-fuel conversion [1], light-emitting diodes (LED) [2, 3], lasers [4–6], photodetectors [7, 8], and recently thermochromics [9] is already underway.

Although rapid progress has been made, many fundamental aspects of halide perovskite materials still remain mysterious. Notable examples include the role of non-stoichiometric starting precursors (small fraction of chloride, acetate, or water content) in the formation of $CH_3NH_3PbI_3$, the origin of the electrical hysteresis seen in many solar cells, and the underlying reason for such high open-circuit voltages and slow recombination in thin-films containing a large density and diversity of defects (vacancies, chemical impurities, grain boundaries, unpassivated surfaces) that in most material systems would be considered of very low quality [10]. Also, because of their promise for large-scale applications such as photovoltaics, stability problems and degradation mechanisms must be well characterized. In these and other remaining puzzles, there is ample room for contributions from scientists and engineers with different backgrounds working in both experiment and theory. While many have chronicled the development of halide perovskite photovoltaic devices, this introduction focuses on the structure and deposition methods, before surveying their unique optical and electrical properties, noting areas that still require further investigation.

1.1.1 Crystal structures

The general formula of the perovskite crystal structure is ABX_3, in which A is the larger cation, B is the smaller cation, and X is the anion. In the most common hybrid-halide perovskites these are, respectively $CH_3NH_3^+$, Pb^{2+}, and a halide (I^-, Br^-, and Cl^-) or mixture of halides. The smaller B cations are octahedrally coordinated by X anions,

with the octahedra sharing corners in a three-dimensional (3D) lattice. The larger *A* cations fill the vacancies between the octahedra and have twelve X nearest neighbors. The possibilities for cation *A* and *B* are limited by the stability of the resulting structure, which can be estimated geometrically by the Goldschmidt tolerance factor and an octahedral factor introduced by Li [11]. Although these two parameters are quite successful in predicting the formation of a perovskite, predicting which distortions occur to the archetypical cubic structure is more difficult because these geometric factors do not account for ionic or covalent-bonding interactions, vibrational motion, or hydrogen bonding. These distortions reduce the symmetry of the lattice into a tetragonal or orthohombic space group, but the distorted perovskite retains the chemical formula and coordination numbers of the archetypical cubic structure.

To determine the structure and space group of perovskite experimentally, X-ray diffraction (XRD) is typically used, but it provides limited information. For example, in $CH_3NH_3PbI_3$, the position of the $CH_3NH_3{}^+$ is determined only indirectly by its effect on the inorganic portion of the crystal. Analyzing the position and orientation of this molecule within the 3D framework is important since alignment of the C-N dipoles is proposed to be the source of ferroelectricity in this materials. The rotational freedom imparts pseudo-spherical symmetry to the $CH_3NH_3{}^+$ which is necessary for a cubic structure [10].

1.1.2 Methods of deposition

One of the key benefits of perovskites is the apparent simplicity of their preparation; however, often a simple procedure belies complex thermodynamics and kinetics that give the material its unique morphology and properties. The $CH_3NH_3PbI_3$ perovskite thin-films have been produced primarly by precipitation from solution: the metal halide and organic halide are dissolved, and spin-coating followed by evaporation yields perovskite thin-films. Additionally, a combination of two-step processes in both solution and vapor phases have been explored as well as fully vapor-phase methods.

Common solvents include Lewis bases such as dimethylformamide (DMF), dimethylsulfoxide (DMSO), and gamma-butyrolactone. Little is known about the species present in solution, although solvents such as DMSO and DMF are known to coordinate to Pb^{2+} halide salts [12–14], and Pb^{2+} halide complexes are common in aqueous solutions of excess halide [15, 16]. The morphology of the resulting films produced from solution depends critically on the choice of solvent(s), the mode of their removal, and also on the substrate's morphology and surface chemistry [17–20, 22, 58]. For example, using DMSO in a mixture of solvents produces an intermediate phase after spincoating that then crystallizes into the perovskite film upon annealing [19]. Addition of a hydrohalic acid into the precursor solution has offered some improvement in the film morphology, but the underlying reason remains unclear [20, 22, 23, 58].

In order to gain better control over the deposition of $CH_3NH_3PbI_3$, a two-step solution process was developed and has in general produced solar cells with higher efficiencies than the single-step process [24], which could be due to the film's different carrier type and doping concentration. In this approach, either PbI_2 or $PbCl_2$ is

dissolved in DMF, spincoated onto a substrate, and then dried into a film. This film is then either dipped into an alcoholic solution of excess CH_3NH_3I alone or a CH_3NH_3I - CH_3NH_3Cl mixture [24, 25] or spincoated repeatedly with such a solution to convert the lead-halide film into the perovskite [26]. When such a process is applied to $PbCl_2$, $CH_3NH_3PbI_3$ is formed, presumably because according to the theory of hard and soft acids and bases [27] the softer, more polarizable I^- has much greater affinity for Pb^{2+} than the much harder Cl^-. As this approach requires diffusion of the $CH_3NH_3{}^+$ cations into the lead-halide matrix, it is possible that there is a thickness limitation on the films formed by this approach or higher temperatures or longer times are required to produce thicker films [28].

Vapor-phase methods produce halide-perovskites with different morphology and crystal structure. Co-evaporation of $PbCl_2$ and CH_3NH_3I in a vacuum deposition chamber yields highly uniform $CH_3NH_3PbI_3$ films with excellent photovoltaic characteristics [30]. The evaporation rates of the precursors determine the composition of the resulting perovskite, and the $CH_3NH_3PbI_3$ produced was confirmed to be cubic rather than the usual tetragonal phase that exists at room temperature.

Table 1.1: Comparison between $CH_3NH_3PbI_3$-based perovskites and other photovoltaic technologies. Perovskites have many of the advantages of polycrystalline semiconductors such as CIGS and CdTe, but they are processed from solution-like organic materials or quantum dots. Material characteristics refer to values measured for materials similar to those used in the highest performing solar cells. This table is adapted from [10] with updated number of column 2; the efficiency[29].

Photovoltaic technology	Power conversion efficiency (%) †	Absorption coefficient (cm^{-1}) ‡	Diffusion length (μm) ♭	Carrier mobility (cm^2/V.s) ♭	Carrier lifetime ♭
c-Si	26.7	10^2	100 - 300	10 - 10^3	4 ms
GaAs (thin-film)	28.8	10^4	1 - 5	>10^3	50 ns
CIGS	22.6	10^3 - 10^4	0.3 - 0.9	10 - 10^2	250 ns
CdTe	21.5	10^3	0.4 - 1.6	10	20 ns
Organic	12.1	10^3 - 10^5	0.005 - 0.01	10^{-5} - 10^{-4}	10-100 μs
Quantum dot	13.4	10^2 - 10^3	0.08 - 0.2	10^{-4} - 10^{-2}	30 μs
Perovskite	22.7	10^3 - 10^4	0.1 - 1.9	2 - 66	270 ns

† under AM1.5 (100 mW/cm^2)
‡ at 300 K in the vicinity of the band edge
♭ of the minority carrier (c-Si, GaAs, CIGS, CdTe, Perovskite) or the mobility of the exciton (Organic, Quantum dot)

1.1.3 Optical properties

Understanding the optical response of halide perovskite thin-films is crucial for optoelectronic applications such as photovoltaics, but it can also provide insight into the electronic and chemical structure.

Although tuning the band gap of perovskites is well documented, a more detailed understanding of these materials's optical properties awaits further research. For instance, dielectric constants in the ultraviolet, visible, and near-IR regions are critical to understanding the optical response of perovskites and also to calculating their absorption and emission properties when incorporated into optoelectronic devices. Progress in this area has been hindered by the difficulty of producing continuous films of sufficient smoothness [31] to avoid measurement artifacts from spectroscopic measurements of reflectance, transmittance, and ellipsometry. Film characterization using ellipsometry usually accounts for remaining surface roughness via modeling to produce the most reliable optical constants possible remains to be independently confirmed. Quantitative absorption coefficients have been determined from the absorption of $CH_3NH_3PbI_3$ on quartz [32], and glass [5], yielding values of 10^4 cm^{-1} near the band edge, but no detailed data of the film's morphology has been provided and no corrections for the surface's inhomogeneity have been applied; consequently, the reported values are only preliminary, but they are consistent with the absorption coefficients calculated based on the optical constants of $CH_3NH_3PbI_3$ [35]. Additionally, the absorption spectrum of $CH_3NH_3PbI_3$ when it is deposited within a mesoscopic template differs from that of perovskite deposited on planar substrates, which has been attributed to changes in the crystallite morphology that affect the optical transition. Band structure calculations indicate that this change in morphology affects the dipole screening of the excitonic transition [36]. Such differences further complicate accurate determination of the absorption coefficient and other optical parameters of perovskite films, so control over the materials properties of perovskites is of the greatest importance for characterization and applications.

The role of excitons in perovskites has been a topic of considerable debate. Recent studies indicate, however, that no significant population of excitons is present in photovoltaics made from $CH_3NH_3PbI_3$, whose excition-binding energy has generally been reported between 20 and 50 meV and is therefore comparable with the thermal energy at room temperature (k_bT = 26 meV) [37, 38]. Although the population of excitons is small in photovoltaics and remains small even at the higher excitation densities required for stimulated emission [38], the excitonic transition significantly enhances the absorption of hybrid perovskites near the band edge; consequently, the electronic band gap taking this into account is 1.65 eV for $CH_3NH_3PbI_3$. The density of excitons and associated effects should be greater in perovskites with higher band gaps, such as $CH_3NH_3PbBr_3$, whose binding energy has been estimated to be between 15 to 40 meV [39, 40].

Photoluminescence (PL) has been observed in perovskites of pure and mixed compositions. PL efficiency depends strongly upon pump fluence. At low excitation intensities, trapping of photogenerated charges competes effectively with direct

radiative recombination of electrons and holes, reducing luminescence [41]. As the excitation increases, these traps are filled and radiative electron-hole recombination dominates. In this regime, studies have confirmed low trap-induced recombination and two-body recombination dynamics over a range of pump intensities [42, 43]. At higher pumping, the PL efficiency falls as Auger recombination becomes more competitive at the higher carrier densities [31, 32, 38]. PL lifetime measurements have been reported for $CH_3NH_3PbI_3$ and $CH_3NH_3PbI_{3-x}Cl_x$, with longer lifetimes exhibited by the latter (3 to 18 ns *versus* 91 to 341 ns). In general, it is difficult to compare lifetimes directly unless they are measured at the same pump fluence, and the wide range of reported lifetimes for each material is likely due to a combination of varying excitation density and synthetic procedures. For solution-processed polycrystalline semiconductors, such lifetimes are surprising especially considering that essentially nothing has been done to reduce recombination at surface or grain boundaries. Considering that the perovskites exhibit clear self-absorption in their PL [38] and lasing spectra [32], it is not surprising that photon recycling has been reported to play an important role in their excited state dynamics when pathways of non-radiative decay are adequetely suppressed [33, 34].

1.1.4 Electrical properties

For solution-processed semiconductors with domain sizes below a few micrometers, halide perovskites exhibit unprecedented carrier transport properties that enable their stellar performance in photovoltaics. Quantitatively characterizing this transport, understanding the materials properties that give rise to it, and developing ways to improve it are all key directions for research.

The intrinsic electrical properties, such as carrier type, concentration, mobility, and diffusion lengths in halide perovskites have exhibited a large range of values often influenced by the method used to prepare the films. Additionally, the lack of smooth and uniform films on which to perform measurements can make the determination of intrinsic electrical properties challenging since conventional techniques often assume the sample exhibits a specific geometry. The carrier type is typically measured using thermoelectric measurement of the Seebeck coefficient, Hall measurement of the conductivity's response to an applied magnetic field, or thin-film transistor's response to a gating electric field. The Seebeck, Hall, and early resistivity measurements on polycrystalline $CH_3NH_3PbI_3$ indicated n-type conductivity, a carrier concentration of $\sim 10^9$ cm^{-3}, and an electron mobility of 66 cm^2/V.s [44]. From Hall measurements, the electron mobility for n-type films deposited from stoichiometric precursors was determined to be 3.9 cm^2/V.s [45] which is in accord with the 8 cm^2/V.s measured using terahertz spectroscopy [46], a technique that usually provides an upper limit because it neglects long-range carrier scattering [45]; however, it is not surprising that the mobility depends strongly on the preparation of the film.

The electron mobility of polycrystalline $CH_3NH_3PbI_3$ films compares favorably to that of films of other materials used as absorbers in solar cells. It is larger than the thin-film mobility of polymers (10^{-7} to 1 cm^2/V.s) [47, 48] and colloidal quantum dots (10^{-3} to 1 cm^2/V.s) [49] and it is comparable with that of CdTe (10 cm^2/V.s) [50],

CIGS and Cu_2ZnSnS_4 (CZTS) (10 to 100 cm^2/V.s) [51, 52] and polycrystalline Si (40 cm^2/V.s) [53]. Even in polycrystalline form, hybrid perovskites's inexpensive processing and tolerance to defects offer a significant advantage over conventional semiconductors.

As is the case for other polycrystalline semiconductors, electrical properties in hybrid perovskites are likely correlated with the film morphology. For instance, the dark and light conductivities of $CH_3NH_3PbI_{3-x}Cl_x$ deposited on a planar scaffold or on mesostructured aluminum oxide are quite different [56]. This difference has been attributed to an increase in the perovskite Fermi level in the mesostructured scaffold either through more surface iodide vacancies or through electrostatic gating from the aluminum oxide. Also, the role of grain boundaries in conduction through perovskite films has not been thoroughly explored, although passivation of grain boundaries with PbI_2 has been correlated to increased radiative lifetimes [57]. Inspired by the literature on organic solar cells, solvent annealing has been applied to $CH_3NH_3PbI_3$ solar cells to increase the grain size of the films to ~ 1 μm [58]. Such processing results in an increase in the photovoltaic performance and radiative lifetime.

1.2 Sources of losses

Generally, materials with a simple processability, such as halide perovskites, would pose a non-negligible level of defects at temperatures relevant for solar cell applications. However, halide perovskite thin-films are considered tolerant to defects [59, 60], relative to conventional semiconductors, and their solar power-conversion-efficiencies already exceed 20 % [61]. Nevertheless, defects still remain one of the critical issues that underpin limitations for further progress of approaching maximum attainable performance. Therefore, with improved engineering methods to control defects, the solar cell power-conversion-efficiencies can be expected to continue approaching the Shockley-Queisser limit [62]. Although theoretical studies of defects have proven useful, experimental confirmation of these results remains paramount. One main obstacle is the inability to identify and decouple the sources of losses. The well-known sources of losses are due to (1) impurities (point defects) and dislocation (line defects) in the bulk, (2) surface imperfections at the front- and back-surfaces, and (3) grain boundaries; all contribute in parallel to the total recombination process of halide-perovskite thin-films [63]. Precise identification of the bulk, surface, and grain boundary effects can help close the gap between our current understanding of defects and their implications for optoelectronic properties, and devices.

1.2.1 Bulk recombination

The bulk recombination occurs via point and line defects. Point defects include vacancy, interstitial, anti-site substitution, Frenkel defect (vacancy and interstitial co-exist at the same ion), and Schottky defect (cation and anion vacancies). While line defects form from dislocation of propagation point defects. These defects are

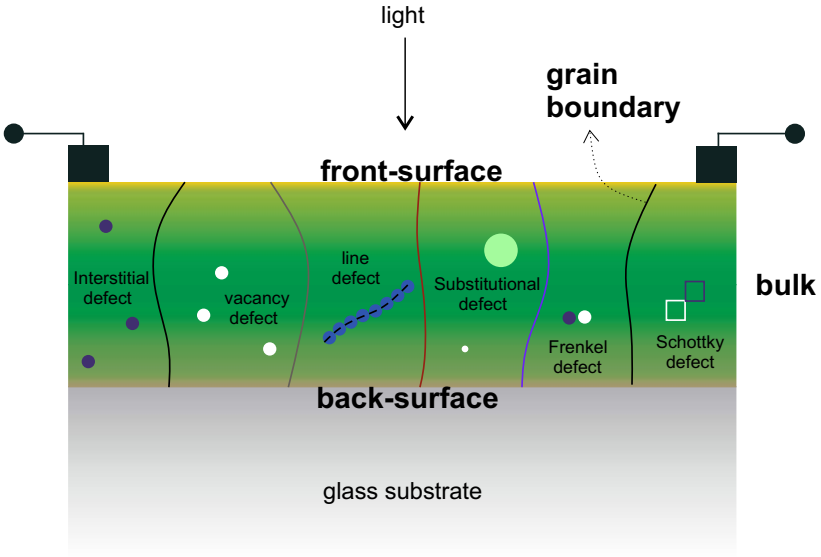

Figure 1.2: Basic topological imperfections showing the source of losses in halide perovskite thin-film: bulk, surfaces, and grain boundary. Each contains different characteristics and types of defects (illustrated by the colors).

thermodynamically favourable within the halide perovskites when their formation energies are negative [59, 60, 63]. Since the formation energies depend on atomic and chemical arrangements of the materials, they can vary under different growth conditions. A high-purity bulk (contains only a few parts per millions of impurities) is typically limited to a high temperature and slow grown process, such as the Czochralski method for monocrystalline silicon [64]. Bulk defects can contribute to several unusual phenomena in halide perovskites, such as ionic migration associated with the device electrical hysteresis [10].

1.2.2 Surface recombination

Interfaces consist of various dangling bonds at terraces, kinks, steps, vacancies, and ad-atoms where all non-radiative recombination can take place [65]. These interfaces can occur between the halide perovskite and air (surface), the substrate, another dielectric layer or with a contact layer. Surface and interface quality often has major implications on final device characteristics (particularly the open-circuit voltage and external quantum-yield). Surface recombination velocity is the standard metric used to assess the electronic quality of the front- and back-surfaces in semiconductors [66]. This recombination increases proportionally to the charge density at the interfaces. In a standard device configuration where the incoming light comes from the top, the highest charge generation rate and therefore highest recombination takes place at the front surface. There are two general strategies to minimize surface recombination: (1) reducing the surface state density, and (2) reducing the minority carrier density at the

surface. The first strategy relies on chemical passivation, for instance, by using an appropriate heterojunction [67], while the second one relies on field effect passivation, created for example by heavily doping the surface [54].

1.2.3 Grain boundary recombination

A misorientation between crystal planes creates a grain boundary. This can occur during a fast crystallization process [68]. Any segregation across the grain boundary induces excess free energy which is used to equilibrate the mechanical strains of the planar defect. In other words, the more grain boundaries, the higher mobility toward deformation [69–71]. Abnormal grain growth can occur if there is a large variation in grain boundary mobility and interfacial energy. Thermodynamic principles allow us to predict the grain boundary energies based on their crystallographic misorientation angles. At low angle, the energy enhances proportionally with misorientation, but then strongly depends on population numbers of the misorientation angles [72]. Although the driving forces for forming grain boundaries are similar to those of bulk and surface defects, the implications can be slightly different. For example, there is no fixed charge at the crystalline grain boundaries, therefore the band bending is solely governed by charges at the interface that can be compensated at much lower injection levels [73]. This leads to a higher recombination rate compared that of the front- or back-surface, where fixed charges can reside in the adjacent dielectric layers [74]. Halide perovskite thin-films contain a large grain boundary density. In conventional semiconductors, such as crystalline silicon, grain boundaries create deep-level defect states that reduce carrier lifetime and mobility. On the other hand, the role of grain boundaries in halide perovskite materials remains unclear, with conflicting reports suggesting they are detrimental, unimportant, or even beneficial [75, 76]. A technique that can be suitably used to identify the grain boundaries in halide perovskites will open a great avenue to engineer numerous types of grain boundaries and understand their correlation with optical and electrical properties.

1.3 Methodology for identifying losses

Bulk, surface, and grain boundary defects occur in all thin-film semiconductors. However, differentiating the losses contributed from each mechanism is not straight forward. This requires complete characterization of the materials system and the ability to independently vary the density of each defect. Experimental results are quite often deceiving, given the sensitivity of halide perovskites to a wide variety of stimuli used in standard characterization techniques (electron/ion beams, laser, electric fields) as well as environmental conditions (humidity, temperature, oxygen). This makes careful and highly controlled experiments that can measure materials properties accurately and reproducibly very important. These material properties then can be used as reliable inputs for modelling and simulations. The methodology used in this thesis attempts to improve our understanding, while pointing the way forward to eliminate the losses, and

finally utilizing this knowledge to design even better performing devices. **Figure 1.3** shows a development cycle of understanding the losses for thin-film halide perovskites.

1.3.1 Modelling can tell everything about solar cells

Solar cells consist of multilayer stacked structures (generally). The losses can be identifed from the interface, contact, and bulk properties. Standard methods use first optical simulations taking into account interference between different layers, or using ray optics if combined with wafer based system such as for perovskite-silicon tandem cells. From optical simulations allow for thickness and geometry optimization to minimize parasitic absorption and reflectance losses: all are useful information for device fabrication. The generation rate obtained from the optical simulation can be used for input into the electrical simulation to solve the drift-diffusion equation in which solar cell performance can be predicted. The system becomes more complex when grain boundaries are considered, as the transport becomes a 3D problem. Grating or nanostructured embedded contacts can add additional complications that require full 3D modelling. Nevertheless, a sufficiently sophisticated model can tell us everything we need to know about the solar cells. Quite often modelling provides useful insights into counterintuitive experimental observations. This is a very important feedback loop to carefully design a clean system for measurements.

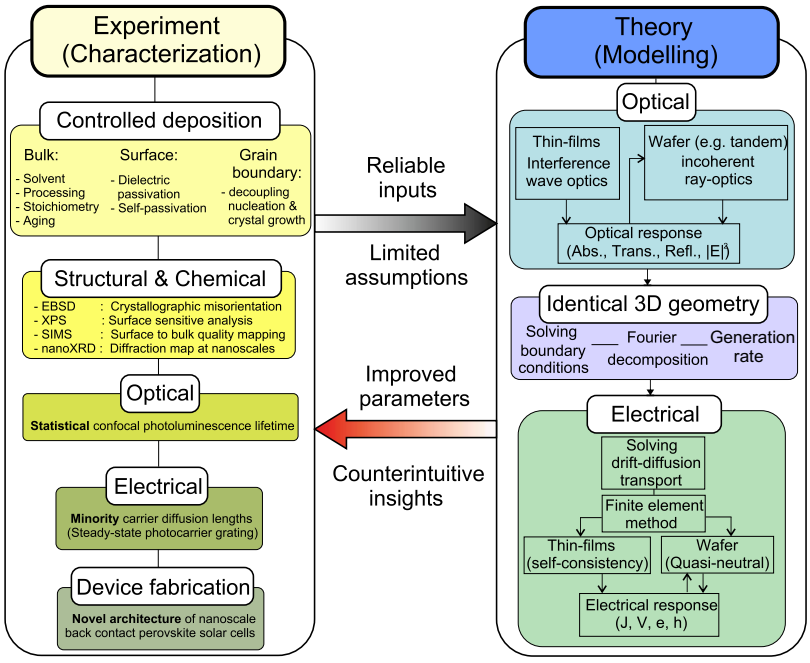

Figure 1.3: The development cycle tool combining experiment and theory to understanding losses in halide perovskite thin-films.

1.3.2 Results are only as accurate as the input and assumptions

The first step to ensure the accuracy from the modelling results is to use appropriate optical constants. One should be aware of the actual condition of the sample from which the optical constant is obtained. For example, very rough surface film could strongly perturb the measured refractive index due to light depolarization during the ellipsometry measurement. Therefore one should implement separetely an effective medium approximation to account for such effects in the input for optical modelling or use smooth films where this is not a problem. For the electrical modelling, it is very important to limit the assumptions being made. In order to extract out the recombination constants from the bulk, surface, and grain boundary, we developed a numerical solution to solve the three-dimensional transport equation using Fourier space. This makes fitting experimental data more efficient, which would otherwise be impossible using computer codes based on a finite element method. The boundary conditions obtained from the Fourier decomposition method can be implemented in our fullly coupled optical-electrical modelling. Instead of modelling a standard device used in the lab, we start by benchmarking our routine for a novel architecture device, such as nanoscale back-contact perovskite-silicon tandem. We considered the most ideal and realistic inputs possible to predict what novel design can beat the current standard device architecture.

1.3.3 What are required for reliable inputs ?

All outputs from the modelling should be aimed to help us understand the experimental results, toward reaching the best possible material and device properties. This process becomes meaningful when inputs obtained from the experiments are reliable. We developed two general strategies approaching that purpose: (1) controlled and clean systems, and (2) careful measurements.

Controlled and clean systems

Unlike silicon semiconductor technology with complex processing but simple structure, halide perovskites display relatively complex chemistry and rich physics given their simple solution deposition. Therefore we develop thin-film deposition protocols to have control over the bulk, surface, and grain size characteristics. Among those the most notable protocol is the deposition method to control grain size without affecting much the bulk and surface quality. This can be achieved by decoupling the nucleation and crystal growth steps. The nucleation is controlled during the spin-coating process from a saturated stock solution. The nucleation sites can stay for extended periods of time, unless heat treatment is applied, at which point crystal growth takes place. The final grain size is inversely proportional to the density of nucleation sites; a lower nucleation density yields larger grains. The density of nucleation sites is controlled by the spin-coating time with fixed spin-speed; longer time yields higher nucleation density. We continuously document our observation, optimize it, and assess the compatibility and limitation of our method. Even if we are able to control the grain size, this still does

not guarantee a perfectly clean system; we observe one peculiar case where amorphous grain boundaries showing unusual optical properties form at a particular spin speed. This makes careful characterization critically important as well.

Careful measurements

The various types of characterization techniques used to understand the sources of losses in halide-perovskite thin films should be directed toward the following considerations: (1) what are the limitations of the techniques? (2) are common artifacts and discrepancies routinely addressed? (3) to what extent are the materials tolerant to external perturbation, e.g electron beam-dose, light-soaking, applied voltage (4) what are the actual conditions, settings, and assumptions governing the chosen characterization techniques? and (5) are well-known principles developed for other semiconductors rigorously applicable for the materials under study here? Addressing all such issues simultaneously can be challenging especially at an early stage, so instead of debate, practice should be taken to advance our understanding toward more solid conclusions.

In order to carefully identify the sources of losses, in this thesis there are two notable routine techniques that we used, namely steady-state photocarrier grating (SSPG), and electron back-scattered diffraction (EBSD). These two methods have already been known in the past to study silicon based thin-films, and now have been successfully used perhaps for the first time in halide perovskite thin-films. SSPG is used to directly quantify the minority carrier diffusion length - one of the properties most strongly correlated with optoelectronic device performance. EBSD is used to identify crystalographic misorientation - therefore grain boundaries - whose effect remains poorly understood in the community. For each utilized technique we systematically report their limitations, important artifacts, methods for analysis corrections, and all possible ambiguous deductions or conclusions. In this way, we hope to streamline progress in the community toward rigorous conclusions about the properties of these exciting new optoelectronic materials and their perspectives for high-performance devices.

1.4 Outline of this thesis

This thesis is aimed to improve our limited understanding of losses in the bulk, on the surface, and at the grain boundaries of halide perovskite semiconductor materials, and top point the way forward to even better performance using novel design. Controlled, clean experimental systems along with careful measurement and full optoelectronic modelling/theory are used as a developing cycle tool to verify, and quantify the losses in halide perovskite thin-films. By quantifying and considering all of the losses, the ultimate goal is directed at designing a novel architecture device that potentially exceeds the performance and relaxes the limitation of traditional solar cell configurations.

In **Chapter 2**, we measure minority carrier diffusion length - a key parameter for

solar cell performance - of halide perovskite thin-films. We describe how controlled processing, composition, aging, and surface passivation correlate to the measured diffusion lengths. We find in pure $CH_3NH_3PbI_3$, the diffusion length is largely dependent on the controlled processing conditions. Next, we partially replace iodide (I) with bromide (Br) and find that surprisingly, the diffusion length increases after aging for 1 month in air. Finally, we use a 4-nm Al_2O_3 passivation layer on the top surface of $CH_3NH_3PbBr_3$, leading to a remarkable increase in diffusion length from 201 nm to 532 nm. The correlation that we have established between basic parameter space and diffusion length offers guidance in how to improve material properties.

In **Chapter 3**, we identify and characterize the grain boundary - an important aspect which is often misidentified - of halide perovskite thin-films. The biggest limiting factor is that a gold standard technique - electron backscattered diffraction (EBSD) - destroys halide perovskite thin films. Therefore identifying the grain boundaries using non-crystallographic techniques is deceiving, leading to conflicting literature reports about their influence. We solve this problem using a solid-state EBSD detector with 6,000 times higher sensitivity than the traditional phosphor screen and camera. We model the characteristics of grain boundary interface energy in $CH_3NH_3PbBr_3$ thin-films, and show that the halide-perovskite grains contain no special boundaries, such as crystal twinning. In addition, we find a peculiar case, where the grain boundary very likely consists of amorphous regions.

In **Chapter 4**, we correlate the information from **Chapter 3** to measure and model the effect of grain size on halide perovskite thin-films - a major challenge in understanding perovskite semiconductors. Correlating true grain size with PL lifetime, carrier diffusion length and mobility, shows that grain boundaries are not benign as is often claimed, but have a recombination velocity of 1670 cm/s, comparable to that of crystalline silicon. However, as with silicon, amorphous perovskite can passivate crystalline boundaries, leading to brighter photoluminescence and longer carrier lifetime without reducing diffusion length. This variable grain boundary character explains the mysteriously long lifetime and record efficiency achieved in small grain halide perovskite thin films, while pointing the way forward to even better performance.

In **Chapter 5**, we use our understanding of the losses to design a novel device architecture - nanoscale back-contact perovskite solar cell to improve tandem efficiency. Using coupled optical-electrical modelling, we optimize this architecture for a planar perovskite-silicon tandem, highlighting the roles of nanoscale contacts to reduce the required perovskite electronic quality such as minority carrier diffusion length. We discuss the advances of our design over the traditionally used two- (2-T) and four-terminal tandem (4-T), and point the way towards further improvements enabled by our design such as surface texturing, surface passivation and photoluminescence outcoupling.

Chapter 1 is partly based upon [10], while **Chapter 2**, and **Chapter 5** are based upon [77], and [78], respectively. Full details are listed at the end of this thesis (Scientific portfolio).

References

[1] J. Luo, J-H. Im, M. T. Mayer, M. Schreier, M. K. Nazeeruddin, N. G. Park, S. D. Tilley, H. J. Fan, and M. K. Grätzel, *Water photolysis at 12.3 % efficiency via perovskite photovoltaics and earth-abundant catalysts*, Science **353**, 1593 (2014).

[2] Z. K. Tan, R. S. Moghaddam, M. L. Lai, P. Docampo, R. Higler, F. Deschler, M. Price, A. Sadhanala, L. M. Pazos, D. Credgington, F. Hanusch, T. Bein, H. J. Snaith, and R. H. Friend, *Bright light-emitting diodes based on organometal halide perovskite*, Nature Nanotech. **9**, 1687 (2014).

[3] Y. H. Kim, H. Cho, J. H. Heo, T. S. Kim, N. Myoung, C-L. Lee, S. H. Im, and T. W. Lee, *Multicolored organic-ionorganic hybrid perovskite light-emitting diodes*, Adv.Mater. **27**, 1248 (2014).

[4] F. Deschler, M. Price, S. Pathak, L. E. Klintberg, D. Jarausch, R. Higler, S. Hu, T. Leijtens, S. D. Stranks, H. J. Snaith, M. Atatu, R. T. Phillips, and R. H. Friend, *High photoluminescence efficiency and optically pumped lasing in solution-processed mixed halide perovskite semiconductors*, J. Phys. Chem. Lett. **5**, 1421 (2014).

[5] B. R. Sutherland, S. Hoogland, M. M. Adachi, C. T. O. Wong, E. H. Sargent, and S. E. T. Al, *Conformal organohalide perovskites enable lasing on spherical resonators*, ACS Nano. **8**, 10947 (2014).

[6] Q. Zhang, S. T. Ha, X. Liu, T. C. Sum, and Q. Xiong, *Room-temperature near-infrared high-q perovskite whispering-gallery planar nanolasers*, Nano Lett. **14**, 5995 (2014).

[7] Y. Lee, J. Kwon, E. Hwang, C-H. Ra, W. J. Yoo, J-H. Ahn, J. H. Park, and J. H. Cho, *High-performance perovskite-graphene hybrid photodetector*, Adv. Mater. **27**, 41 (2014).

[8] L. Dou, Y. M. Yang, J. You, Z. Hong, W-H. Chang, G. Li, and Y. Yang, *Solution-processed hybrid perovskite photodetectors with high detectivity*, Nature Comm. **5**, 5404 (2014).

[9] J. Lin, M. Lai, L. Dou, C. S. Kley, H. Chen, F. Peng, J. Sun, D. Lu, S. A. Hawks, C. Xie, F. Cui, A. P. Alivisatos, D. T. Limmer, and P. Yang, *Thermochromic halide perovskite solar cells*, Nature Mat. **5**, 1476 (2018).

[10] S. Brittman, G. W. P. Adhyaksa, and E. C. Garnett *The expending world of hybrid perovskites: materials properties and emerging applications*, MRS Comm. **3**, 7 (2015).

[11] C. Li, X. Lu, W. Ding, L. Feng, Y. Gao, and Z. Guo *Formability of ABX_3 (X = F, Cl, Br, I) halide perovskites*, Acta Crystallogr. B **64**, 702 (2008).

[12] I. Wharf, T. Gramstad, R. Makhija, and M. Onyszchuk *Synthesis and vibrational spectra of some lead(II) halide adducts with O-, S-, and N-donor atom ligands*, Can. J. Chem. **54**, 3430 (1976).

[13] R. J. Alvarado, J. M. Rosenberg, A. Andreu, J. C. Bryan, W-Z. Chen, T. Ren, and K. Kavallieratos *Structural insights into the coordination and extraction of Pb(II) by disulfonamide ligands derived from o-phenylenediamine*, Inorg. Chem. **44**, 7951 (2005).

[14] I. Persson, K. Lyczko, D. Lundberg, L. Eriksson, and A. Paczek *Coordination chemistry study of hydrated and solvated lead(II) ions in solution and solid state*, Inorg. Chem. **50**, 1058 (2011).

[15] G. P. Haight and J. R. Peterson*Chloro complexes of lead(II)*, Inorg. Chem. **4**, 1073 (1965).

[16] H. L. Clever and F. J. Johnston*The solubility of some sparingly soluble lead salts: an evaluation of the solubility in water and aqueous electrolyte solution*, J. Phys. Chem. Ref. Data **9**, 751 (1980).

[17] D. B. Mitzi*Solution-processed inorganic semiconductors*, J. Mater. Chem. **14**, 2355 (2004).

[18] G. E. Eperon, V. M. Burlakov, P .Docampo, A. Goriely, and H. J. Snaith*Morphological control for high performance, solution-processed planar heterojunction perovskite solar cells*, Adv. Funct. Mater. **24**, 151 (2014).

[19] N. J. Jeon, J. H. Noh, Y. C. Kim, W. S. Yang, S. Ryu, and S. Il. Seok*Solvent engineering for high-performance inorganic-organic hybrid perovskite solar cells*, Nature Mater. **13**, 897 (2014).

[20] J. H. Heo, D. H. Song, and S. H. Im*Planar $CH_3NH_3PbBr_3$ hybrid solar cells with 10.4% power conversion efficiency, fabricated by controlled crystallization in the spin-coating process*, Adv. Mater. **26**, 8179 (2014).

[21] Z. Xiao, Q. Dong, C. Bi, Y. Shao, Y. Yuan, and J. Huang*Solvent annealing of perovskite-induced crystal growth for photovoltaic-device efficiency enhancement*, Adv. Mater. **26**, 6503 (2014).

[22] J-H. Im, I-H. Jang, N. Pellet, M. Grätzel, and N-G. Park*Growth of $CH_3NH_3PbI_3$ cuboids with controlled size for high-efficiency perovskite solar cells*, Nature Nano. **9**, 927 (2014).

[23] G. E. Eperon, S. D. Stranks, C. Menelaou, M. B. Johnston, L. M. Herz, and H. J. Snaith*Formamidinium lead trihalide: a broadly tunable perovskite for efficient planar heterojunction solar cells*, Energy Environ. Sci. **7**, 982 (2014).

[24] J. Burschka, N. Pellet, S-J. Moon, R. Humphry-Baker, P. Gao, M. K. Nazeeruddin, and M.Grätzel*Sequential deposition as a route to high-performance perovskite-sensitized solar cells*, Nature **499**, 316 (2013).

[25] P. Docampo, F. Hanusch, S. D. Stranks, M. Döblinger, J. M. Feckl, M. Ehrensperger, N. K. Minar, M. B. Johnston, H. J. Snaith, and T. Bein*Solution deposition-conversion for planar heterojunction mixed halide perovskite solar cells*, Adv. Energy Mater. **4**, 1400355 (2014).

[26] Y. Kutes, L. Ye, Y. Zhou, S. Pang, B. D. Huey, and N. P. Padture*Direct observation of ferroelectric domains in solution-processed $CH_3NH_3PbI_3$ perovskite thin films*, J. Phys. Chem. Lett. **5**, 3335 (2014).

[27] R. G. Pearson *Hard and soft acids and bases*, J. Chem. Educ. **45**, 581 (1968).

[28] N. Kitazawa, Y. Watanabe, and Y. Nakamura *Optical properties of $CH_3NH_3PbX_3$ (X = halogen) and their mixed-halide crystals*, J. Mater. Sci. Soc. **7**, 3585 (2002).

[29] A. Polman, M. Knight, E. C. Garnett, B. Ehrler, and W. C. Sinke *Photovoltaic materials ? present efficiencies and future challenges*, Science **352**, 307 (2016).

[30] M. Liu, M. B. Johnston, and H. J. Snaith *Efficient planar heterojunction perovskite solar cells by vapour deposition*, Nature **501**, 395 (2013).

[31] T. C. Sum and N. Mathews *Advancements in perovskite solar cells: photophysics behind the photovoltaics*, Energy Environ. Sci. **7**, 2518 (2014).

[32] G. Xing, N. Mathews, S. S. Lim, N. Yantara, X. Liu, D. Sabba, M.Grätzel, S. Mhaisalkar, and T. C. Sum *Low-temperature solution-processed wavelength-tunable perovskites for lasing*, Nature Mater. **13**, 476 (2014).

[33] L. M. Pazos-Outon, M. Szumilo, R. Lamboll, J. M. Richter, M. Crespo-Quesada, M. Abdi-Jalebi, H. J. Beeson, M. Vrucinic, M. Alsari, H. J. Snaith, B. Ehrler, R. H. Friend, and F. Deschler *Photon recyling in lead iodide perovskite solar cells*, Science **351**, 1430 (2016).

[34] J. M. Richter, M. Abdi-Jalebi, A. Sadhanala, M. Tabachnyk, J. P. H. Rivett, L. M. Pazos-Outon, K. C. Godel, M. Price, F. Deschler, and R. H. Friend *Photon reabsorption masks intrinsic bimolecular charge-carrier recombination in $CH_3NH_3PbI_3$ perovskite*, Nature Comm. **8**, 13941 (2016).

[35] M. Stuckelberger, B. Niesen, M. Filipic, S. Moon, J. Yum, M. Topic, and C. Ballif *Complex refractive index spectra of $CH_3NH_3PbI_3$ perovskite thin films determined by spectroscopic ellipsometry and spectrophotometry*, Phys. Chem. Lett. **6**, 66 (2015).

[36] J. Even, L. Pedesseau, J-M. Jancu, and C. Katan *Importance of spin-orbit coupling in hybrid organic/inorganic perovskites for photovoltaic applications*, Phys. Chem. Lett. **4**, 2999 (2013).

[37] V. D'Innocenzo, G. Grancini, M. J. P. Alcocer, A. R. S. Kandada, S. D. Stranks, M. M. Lee, G. Lanzani, H. J. Snaith, and A. Petrozza *Excitons versus free charges in organo-lead tri-halide perovskites*, Nature Comm. **5**, 3586 (2014).

[38] M. Saba, M. Cadelano, D. Marongiu, F. Chen, V. Sarritzu, N. Sestu, C. Figus, M. Aresti, R. Piras, A. Geddo-Lehmann, C. Cannas, A. Musinu, F. Quochi, A. Mura, and G. Bongiovanni *Correlated electron-hole plasma in organometal perovskites*, Nature Comm. **5**, 5049 (2014).

[39] K. Tanaka, T. Takahashi, T. Ban, T. Kondo, K. Uchida, and N. Miura *Comparative study on the excitons in lead-halide-based perovskite-type crystals $CH_3NH_3PbBr_3$ and $CH_3NH_3PbI_3$*, Solid State Commun. **127**, 619 (2003).

[40] D. Guo, D. Bartesaghi, H. Wei, E. M. Hutter, J. Huang, and T. J. Savenije *Photoluminescence from radiative surface states and excitons in methylammonium lead bromide perovskites*, J.Phys.Chem.Lett. **8**, 4258 (2017).

[41] S. D. Stranks, V. M. Burlakov, T. Leijtens, J. M. Ball, A. Goriely, and H. J. Snaith *Recombination kinetics in organic-inorganic perovskites: excitons, free charge, and subgap states*, Phys. Rev. Appl. **2**, 034007 (2014).

[42] C. Wehrenfennig, M. Liu, H. J. Snaith, M. B. Johnston, and L. M. Herz *Homogeneous emission line broadening in the organo lead halide perovskite $CH_3NH_3PbI_3$*, J. Phys. Chem. Lett. **5**, 1300 (2014).

[43] J. S. Manser and P. V. Kamat *Band filling with free charge carriers in organometal halide perovskites*, Nature Photon. **8**, 737 (2014).

[44] C. C. Stoumpos, C. D. Malliakas, and M. G. Kanatzidis *Semiconducting tin and lead iodide perovskites with organic cations: phase transitions, high mobilities, and near-infrared photoluminescent properties*, Inorg. Chem. **52**, 9019 (2013).

[45] Q. Wang, Y. Shao, H. Xie, L. Lyu, X. Liu, Y. Gao, and J. Huang *Qualifying composition dependent p and n self-doping in $CH_3NH_3PbI_3$*, Appl. Phys. Lett. **105**, 163508 (2014).

[46] C. Wehrenfennig, G. E. Eperon, M. B. Johnston, H. J. Snaith, and L. M. Herz *High charge carrier mobilities and lifetimes in organolead trihalide perovskites*, Adv. Mater. **26**, 1584 (2014).

[47] D. Venkateshvaran, M. Nikolka, A. Sadhanala, V. Lemaur, M. Zelazny, M. Kepa, M. Hurhangee, A. J. Kronemeijer, V. Pecunia, I. Nasrallah, I. Romanov, K. Broch,

I. McCulloch, D. Emin, Y. Olivier, J. Cornil, D. Beljonne, and H. Sirringhaus *Approaching disorder-free transport in high-mobility conjugated polymers*, Nature **515**, 384 (2014).

[48] J. You, L. Dou, Z. Hong, G. Li, and Y. Yang *Recent trends in polymer tandem solar cells research*, Polym. Sci. **38**, 1909 (2013).

[49] C. S. S. Sandeep, S. Cate, J. M. Schins, T. J. Savenije, Y. Liu, M. Law, S. Kinge, A. J. Houtepen, and L. D. A. Siebbeles *High charge-carrier mobility enables exploitation of carrier multiplication in quantum-dot films*, Nature Comm.**4**, 2360 (2013).

[50] Q. Long, S. A. Dinca, E. A. Schiff, M. Yu, and J. Theil *Electron and hole drift mobility measurements on thin film CdTe solar cells*, Appl. Phys. Lett.**105**, 042106 (2014).

[51] B. Shin, O. Gunawan, Y. Zhu, N. A. Bojarczuk, S. J. Chey, and S. Guha *Thin film solar cell with 8.4% power conversion efficiency using an earth-abundant Cu_2ZnSnS_4 absorber*, Prog. Photovolt. Res. Appl.**21**, 72 (2013).

[52] G. Brown, V. Faifer, A. Pudov, S. Anikeev, E. Bykov, M. Contreras, and J. Wu *Determination of the minority carrier diffusion length in compositionally graded $Cu(In,Ga)Se_2$ solar cells using electron beam induced current*, Appl. Phys. Lett.**96**, 022104 (2010).

[53] T. I. Kamins *Hall mobility in chemically deposited polycrystalline silicon*, J. Appl. Phys. **42**, 43574365 (1971).

[54] M. A. Green , *Silicon Solar Cells Advanced Principles and Practice*, UNSW Photovoltaics, Sydney, 1995.

[55] J. S. Blakemore *Semiconducting and other major properties of gallium arsenide*, J. Appl. Phys. **53**, 123 (1982).

[56] T. Leijtens, S. D. Stranks, G. E. Eperon, R. Lindblad, E. M. J. Johansson, J. M. Ball, M. M. Lee, H. J. Snaith, and I. J. McPherson *Electronic properties of meso-superstructured and planar organometal halide perovskite films: charge trapping, photodoping, and carrier mobility*, ACS Nano **8**, 7147 (2014).

[57] Q. Chen, H. Zhou, T-B. Song, S. Luo, Z. Hong, H-S. Duan, L. Dou, Y. Liu, and Y. Yang *Controllable self-induced passivation of hybrid lead iodide perovskites toward high performance solar cells*, NanoLett. **14**, 4158 (2014).

[58] Z. Xiao, Q. Dong, C. Bi, Y. Shao, Y. Yuan, and J. Huang *Solvent annealing of perovskite-induced crystal growth for photovoltaic-device efficiency enhancement*, Adv.Mater.**26**, 6503 (2014).

[59] W-J. Yin, T. Shi, and Y. Yan, *Unusual defect physics in $CH_3NH_3PbI_3$ perovskite solar cell absorber*, Appl.Phys.Lett. **104**, 4 (2014).

[60] A. Walsh, D. O. Scanlon, S. Chen, X. G. Gong, and S-H. Wei, *self-regulation mechanism for charged point defects in hybrid halide perovskites*, Angew. Chem. Int. Ed. **54**, 1791 (2015).

[61] M. A. Green, Y. Hishikawa, E. D. Dunlop, D. H. Levi, J. H-Ebinger, and A. W. Y. Ho-Baillie *Solar cell efficiency tables (version 51)*, Prog.in Photovolt. **26**, 3 (2018).

[62] W. Shockley and H. J. Queisser *Detailed balance limit of efficiency of p-n junction solar cells*, J.Appl. Phys. **31**, 510 (1961).

[63] J. M. Ball and A. Petrozza *Defects in perovskite-halides and their effects in solar cells*, Nature Energy **1**, 16149 (2016).

[64] T. Nishinaga, *Handbook of Crystal Growth: Fundamentals*, Elsevier, Amsterdam, 2015.

[65] G. A. Somorjai and Y. Li , *Introduction to Surface Chemistry and Catalysis*, Wiley-Interscience, New Jersey, 2010.

[66] Y. Yang, M. Yang, D. T. Moore, Y. Yan, E. M. Miller, K. Zhu, and M. C. Beard *Top and bottom surface limit carrier lifetime in lead iodide perovskite films*, Nature Energy **2**,

16207 (2017).

[67] G. Dingemans and W. M. M. Kessels *Status and prospects of Al_2O_3 based surface passivation schemes for silicon solar cells*, J. Vac. Sci. Tech. A Vacuum, Surface, Film **30**, 40802 (2012).

[68] A. P. Sutton and R. W. Balluffi, *Interfaces in Crystalline Materials*, Clarendon Press, Oxford, 1998.

[69] B. L. Adams, S. Ta'asan, D. Kinderlehrer, I. Livshits, D. E. Mason, C-T, Wu, W. W. Mullins, G. S. Rohrer, A. D. Rollett, and D. M. Saylor, *Extracting grain boundary and surface energy from measurement of triple junction geomtery*, Interface Science **7**, 321 (1999).

[70] Y. Huang and F. J. Humphreys, *Measurement of grain boundary mobility during recrystallization of a single-phase aluminium alloy*, Acta Materialia **47**, 2259 (1999).

[71] M. Taheri, H. Weiland, and A. Rollett, *Method of measuring stored energy macroscopically using statistically stored dislocations in commercial purity aluminum*, Metall. and Mat. Trans. A **37**, 19 (2006).

[72] W. T. Read and W. Shockley, *Dislocation models of crystal grain boundaries*, Phys. Rev. **78**, 275 (1950).

[73] J. Nelson, *The Physics of Solar Cells*, Imperial Collage Press, London, 2003.

[74] R. Brendel, *Thin-Film Crystalline Silicon Solar Cells Physics and Technology*, Willey-VCH Verlag GmbH, Weinheim, 2003.

[75] J. S. Yun, A. Ho-Baillie, S. Huang, S. H. Woo, Y. Heo, J. Seidel, F. Huang, Y-B. Cheng, and M. A. Green, *benefit of grain boundaries in organic-inorganic halide planar perovskite solar cells*, J.Phys.Chem.Lett. **6**, 875 (2015).

[76] D. W. deQuilettes, S. M. Vorpahl, S. D. Stranks, H. Nagaoka, G. E. Eperon, M. E. Ziffer, H. J. Snaith, D. S. Ginger, *Impact of microstructure on local carrier lifetime in perovskite solar cells*, Science **348**, 683 (2015).

[77] G. W. P. Adhyaksa, L. W. Veldhuizen, Y. Kuang, S. Brittman, R. E. I. Schropp, and E. C. Garnett, *Carrier diffusion lengths in hybrid perovskites: processing, composition, aging, and surface Passivation Effects*, Chem. Mater. **28**, 5 (2016).

[78] G. W. P. Adhyaksa, E. Johlin, and E. C. Garnett, *Nanoscale Back Contact Perovskite Solar Cell Design for Improved Tandem Efficiency*, Nature Lett. **17**, 7 (2017).